# Numerical Analysis of Passive Piles under Surcharge Load in Extensively Deep Soft Soil

Meixiang Gu [ID], Xiaocong Cai, Qiang Fu *[ID], Haibo Li, Xi Wang and Binbing Mao

School of Civil Engineering, Guangzhou University, Guangzhou 510006, China
* Correspondence: cefuqiang@gzhu.edu.cn

**Abstract:** The three-dimensional finite difference method was used in this study to analyze the deformation and stresses of a passive pile under surcharge load in extensively deep soft soil. A three-dimensional numerical model was proposed and verified by a field test. The horizontal displacements of the pile agreed well with the field results. This study investigated the pile-foundation soil interaction, the load transfer mechanism, the excess pore water pressure (EPWP), and the horizontal resistance of the foundation soil. The results show that the soil in the corner of the loading area developed a large uplift deformation, while the center of the loading area developed a large settlement. The lateral displacement of the pile decreased sharply with the increase of the depth and increased with the surcharge load. The lateral displacement of the soil was negligible when the depth exceeded 30 m. The EPWP increased in a nonlinear way with the increase of the surcharge load and accumulated with the placement of the new lift. The distribution of the lateral earth pressure in the shallow soil layer was complex, and the negative value was observed under a high surcharge load due to the suction effect. The proportion coefficient of the horizontal resistance coefficient showed much smaller value in the situation of large lateral deformation and high surcharge load. The design code overestimated the horizontal resistance of the shallow foundation soil, which should be given attention for the design and analysis of the laterally loaded structures in extensively soft soil.

**Keywords:** passive pile; surcharge load; horizontal resistance; extensively soft soil; pile-soil interaction

## 1. Introduction

Pile foundations have been extensively used in soft soil to support bridges, buildings, and highways. The active pile has in general carried the vertical (e.g., superstructure) and lateral (e.g., wind) loads, which were imposed onto the pile head. Such loads were considered in the initial design for the active pile. In some situations, the pile foundation was also subject to the soil movement resulting from adjacent surcharge loading [1], excavation [2], and landslide [3], known as the passive-pile. Several studies [4–9] have been conducted to investigate the response of the passive pile under adjacent surcharge loading. They concluded that the motion effect of the soil acting on the pile would result in large deformations or even failure of the structure. The failure of such piles was usually governed by the lateral deformation, which was different from the design of the active pile. However, the pile-foundation soil interaction was an extraordinarily complex topic due to the soil movement induced by adjacent surcharge loading.

In recent decades, researchers have conducted laboratory tests [10–17] and theoretical calculations [12,16,18–21] to understand the characteristics of pile foundation-soil interaction. However, the mechanism of pile-soil interactions due to lateral soil movement still lacks clarity. Most theoretical methods for prediction have not been validated due to the lack of field test data, which resulted in passive features being often neglected in the design [22]. Tavenas, et al. [23] established the least-square regression prediction model based on 21 different embankments tests. They concluded that the lateral deformation at the end of construction was hard to predict. The neglect of initial consolidation could cause the

failure of the previous prediction of lateral displacements during construction. Poulos [24] found that the predicted horizontal displacement showed considerable inconsistency with the measured data, based on summarized cases. Despite all this, the field data were usually of great value, e.g., they could be used to check the authenticity of the pile-soil interaction. Li, et al. [25] pointed out that field tests could coincide more with the real condition and reflect the actual behavior of the piles subject to adjacent surcharge loading, though those tests were expensive and time-consuming.

Nicu, et al. [26] measured the abutment pile foundation built on 13.5 m of thick hard clay in the field. They gave the limit value of the abutment. Ong, et al. [27] proposed an empirical equation for estimating the maximum net lateral displacement in the preliminary design based on 18 field cases. However, it was difficult to provide totally reliable data and conclusions through laboratory and field tests because the soil characteristics and the superstructure were complex. Numerical analysis [10,28] has become a favorite method for solving such problems. Yang, et al. [29] employed two different modeling methods verified by field tests to simulate the pile-soil interaction. Their results demonstrated that a larger loading rate usually led to a higher earth pressure on the front pile. Al-abboodi and Sabbagh [30] applied the commercial software (PLAXIS 3D) to analyze the passive piles. They concluded that there were some differences between the test and predicted results because the relative lateral displacement of pile-soil was not considered. Zhang and Sun [31] investigated the influence of landfill loading on the bridge pile foundation near the expressway using the finite element method (FEM). Abo-Youssef, et al. [32] used the three-dimensional FEM to study the behavior of the abutment pile and considered the secondary consolidation of the soil. They found that the secondary compression had a slight effect on the maximum moment value and the lateral soil movement was time dependent.

This paper employed the three-dimensional finite difference method to analyze the deformation and stresses of a passive pile under a surcharge load in extensively deep soft soil. The numerical model was verified by the corresponding field test reported by Yi, et al. [33]. The pile foundation-soil interaction, the load transfer mechanism, the excess pore water pressure (EPWP), and the horizontal resistance of the foundation soil were investigated in this study.

## 2. Field Test

The project site was in Zhongshan City, Guangdong Province, China. Extensively soft soil stratum was widely distributed in this coastal area. The thickness of the soft soil layer could reach 35–40 m. The marine deposit was composed of the sea-land sedimentary silt and mud layers. The thickness of the sea-land sedimentary silt layer was 5.2 m. The cohesion and friction angle of the silt were 8.4 kPa and 0.5 degrees based on laboratory tests. The thickness of the mud layer was 31.8 m. The cohesion and friction angle of the mud were 13.6 kPa and 6.8 degrees. A new highway was designed to cross this region, which was composed of ponds, farmland, and rivers. Reinforced concrete pile foundations with elevated caps were designed for the bridge to cross the extensively deep soft soil in this region. On the other hand, the interchange ramp was designed at some locations and was close to the existing bridge foundation. The interchange ramp was constructed by a 4 m thick embankment, and it led to high lateral loads on the adjacent pile foundation. Apparently, the newly built subgrade would affect the existing piles and result in settlement, displacement, and even failure of the pile foundations [34].

Therefore, a field test was carried out using a single steel pipe pile with a diameter of 630 mm and a length of 35 m to investigate the behavior of the existing pile under newly placed surcharge loads. The steel pipe pile was used to simulate the reinforced concrete pile for the bridge foundation in the field. The open-ended steel pipe pile penetrated the soft soil using the vibrosinking method. An embankment with the thickness of 4 m was constructed in 5 lifts. Each lift was placed with the 0.8 m thick soil and maintained for 3 days until the placement of the next lift. Figure 1 shows the construction sequence of the surcharge. The embankment fill was distributed within a rectangle zone (e.g., 16 m

in width and 24 m in length). The slope gradient of the embankment was kept at 1:1.5. The surcharge load was calculated as the gravity of the embankment fill divided by the loading area (e.g., 16 m × 24 m = 384 m$^2$). Figure 2 shows the layout of the field test and the positions calculated in the numerical model, which included the profile view, plan view, and the instrumentations. The detailed information of the field test and the measurement results can be found in Yi, et al. [33] and was not introduced in here for purposes of brevity.



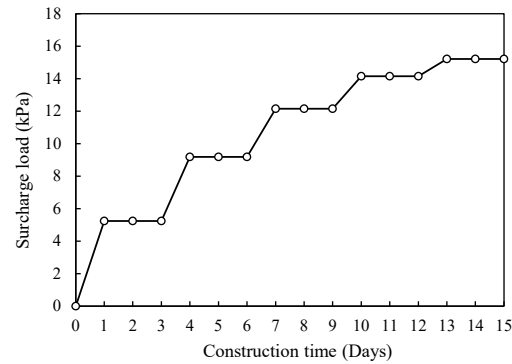**Figure 1.** The surcharge load versus the construction time in the field and the numerical analysis.
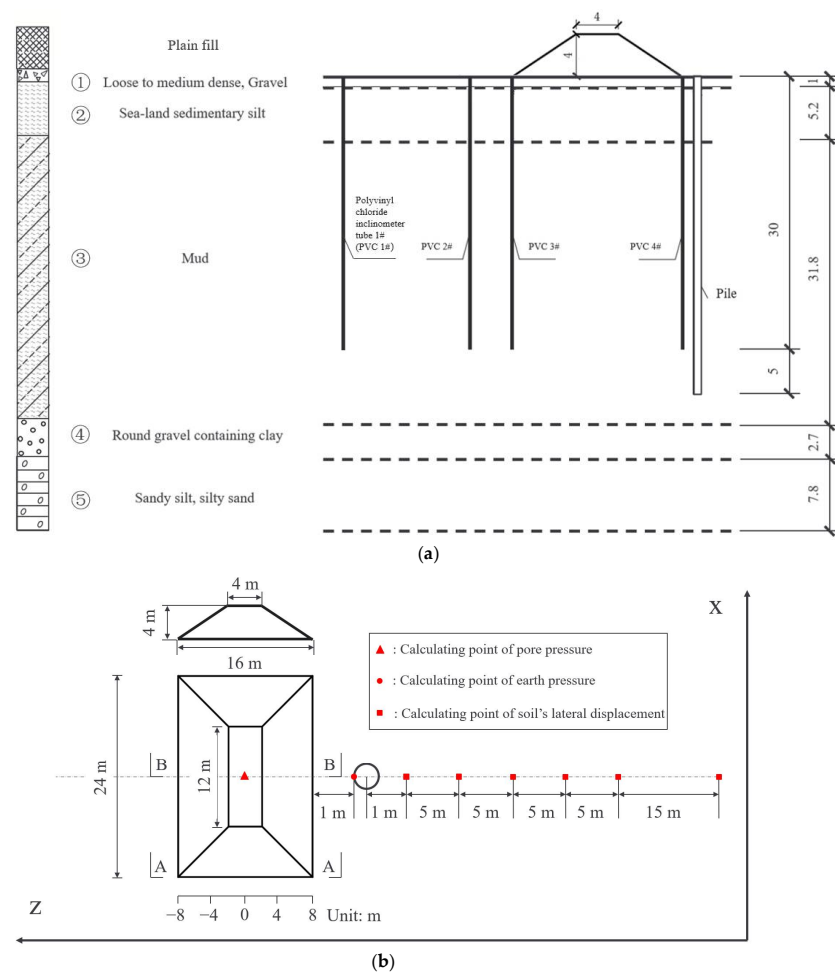


**Figure 2.** The layout of the field test and the positions calculated in the numerical model: (**a**) profile view; (**b**) plan view. (Unit: m).

## 3. Numerical Modelling

### 3.1. General

The three-dimensional Fast Lagrangian Analysis of Continuum (FLAC3D, Itasca [35]) was used in this paper to study the performance of a single pile installed in an extensively soft soil layer under surcharge loading. The numerical method can solve complex geotechnical problems for three-dimensional analysis of slope stability, earthquake simulations, and underground excavation. The large-strain simulation was used and node locations were updated during each calculation cycle to capture the full extent of pile and soil deformations. The displacements and forces were solved numerically using an explicit finite difference formulation in time. The proposed numerical model was calibrated against the field test results. Figure 3 shows the schematic diagram of the numerical model, which included the profile view and the plan view. The three-dimensional size of the numerical model was determined as 46 m in width, 50 m in depth, and 162.63 m in length. The normal velocity of the foundation soil's bottom and side surfaces was fixed to zero to simulate the actual boundary conditions in the field situation. The 37 m thick, soft soil was divided into six layers in the numerical model to capture the actual soil properties. The thickness of each layer was 2 m, 3 m, 2 m, 3 m, 10 m, and 17 m, respectively, from the top to the bottom layers. The mesh created for the pile and surcharge zone was densified. The total number of 48,208 elements was created in the FLAC3D model.
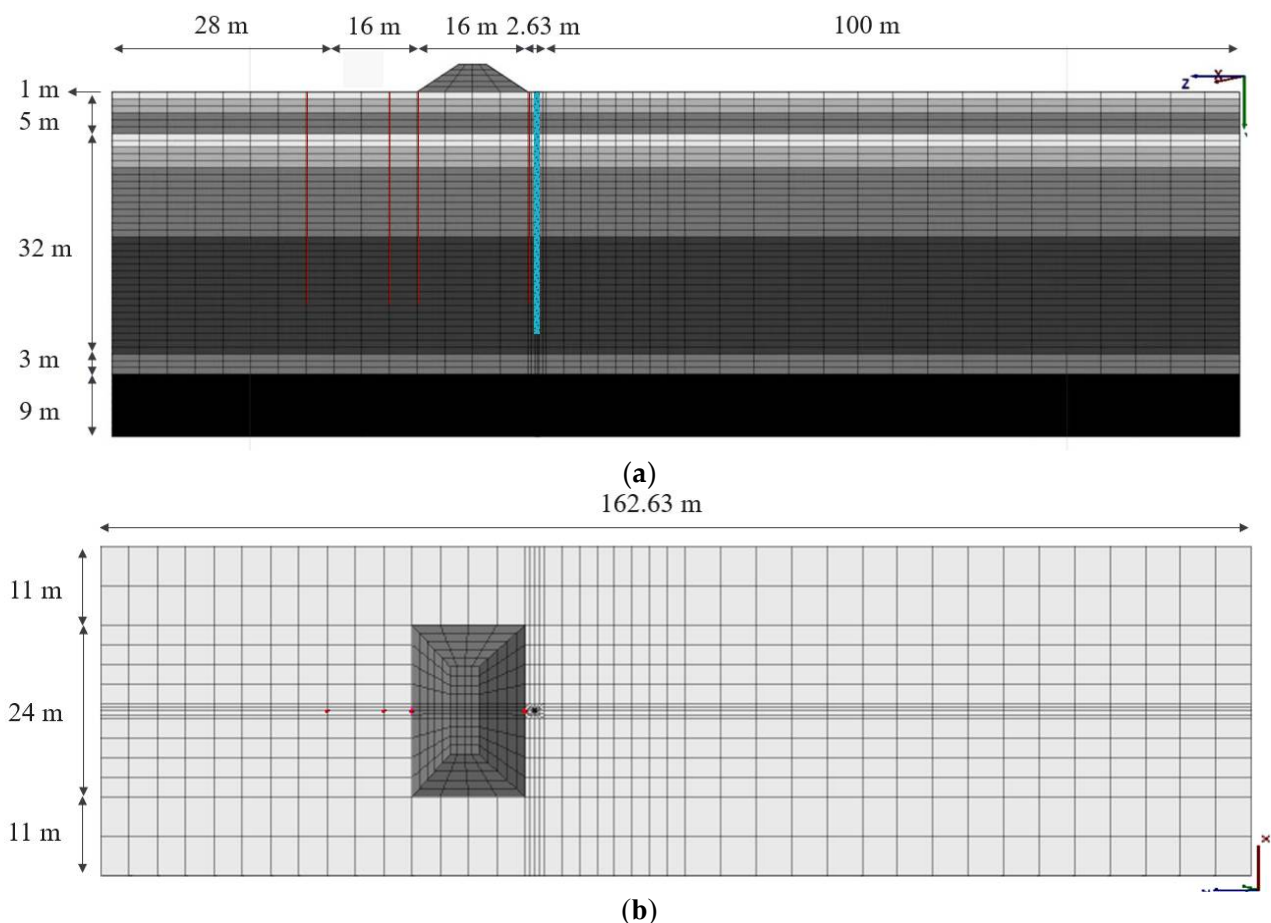


**Figure 3.** The mesh layout of the numerical model: (**a**) profile view; and (**b**) plan view.

In the field construction, the 35 m long steel pipe pile was welded by three short steel pipes. As shown in Figure 4, the mechanical strength of the welding joints was weakened. The bending stiffness of the pile decreased at the welding zone due to the construction

defect. The effect of the welding joints was considered in the numerical model by reducing Young's modulus of the welding zone to $2.0 \times 10^9$ Pa.
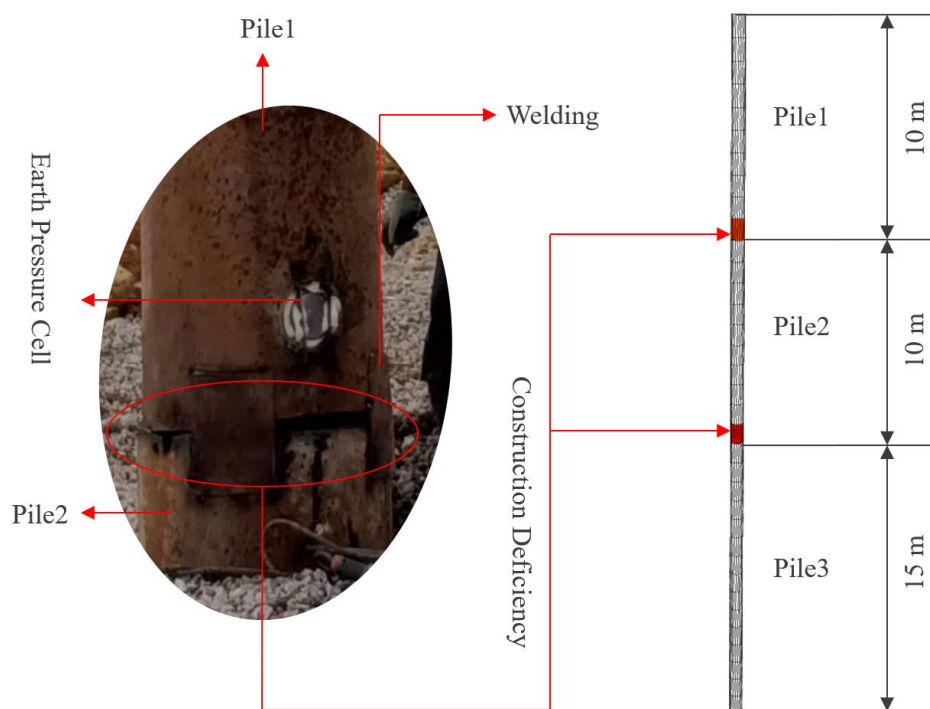


**Figure 4.** The schematic diagram of the welding joints of the steel pipe pile.

### 3.2. Soil and Structure Properties

The soil, steel pipe pile, and inclinometer tube were simulated using the zone-type, shell-type, and pile-type elements, respectively. The shell-type element can reflect the actual geometric size of the steel pipe pile and be used in the numerical model. The material properties were determined based on experimental test results [33] and are summarized in Table 1. The Mohr-Coulomb constitutive model was used to model the 1st, 4th, and 5th soil layers of gravel, sandy silt, and silty sand. The Drucker-Prager model was used to model the 2nd and 3rd soil layers of sea-land sedimentary silt and mud. The steel pipe pile and the inclinometer tube were modeled as elastic materials. The external and internal diameters of the steel pipe pile were 0.63 and 0.62 m, respectively.

**Table 1.** Material parameter.

| Materials | Cohesion (kPa) | Friction Angle (°) | Density (g/cm$^3$) | Young's Modulus (Pa) | Poisson | Constitutive Model |
|---|---|---|---|---|---|---|
| 1st layer | 0 | 37 | 1.65 | $1.0 \times 10^7$ | 0.37 | Mohr-Coulomb |
| 2nd layer | 8.81 | 0.06 | 1.59 | $1.5 \times 10^6$ | 0.45 | |
| | 8.81 | 0.07 | 1.59 | $1.6 \times 10^6$ | 0.45 | |
| | 5.46 | 0.08 | 1.69 | $8 \times 10^6$ | 0.30 | Drucker-Prager |
| 3rd layer | 7.46 | 0.12 | 1.69 | $9 \times 10^6$ | 0.30 | |
| | 10.46 | 0.20 | 1.69 | $1 \times 10^7$ | 0.30 | |
| | 20.46 | 0.45 | 1.69 | $2 \times 10^7$ | 0.30 | |
| 4th layer | 3.0 | 32 | 2.05 | $5.2 \times 10^8$ | 0.30 | |
| 5th layer | 60 | 45 | 2.25 | $1 \times 10^9$ | 0.30 | Mohr-Coulomb |
| Steel pipe pile | - | - | - | $2.0 \times 10^{11}$ | 0.31 | Elastic |
| Inclinometer tube | - | - | - | $4.28 \times 10^8$ | 0.30 | Elastic |

The foundation soil and structure elements (e.g., the steel pipe pile and the inclinometer tube) were generated first and initially reached force balance under gravity. The effect of the underground water was then introduced by setting the water table at 1 m below the ground surface, which was consistent with the actual water table in the field test. The fluid command was activated in the numerical model, and the permeability (isotropy), fluid density, fluid-modulus, and porosity were assigned for the foundation soil. Since no additional drainage method was used during the field test, the water table was set to the drainage surface (i.e., the shallow gravel soil layer). The pore water pressure at the bottom surface of the 1st layer was fixed to zero in the numerical model. The fluid-density, fluid-modulus, and porosity were determined as 1000 kg/m$^3$, $2.18 \times 10^9$ Pa, and 0.60, respectively. The permeability of the 2nd, 3rd, 4th, and 5th soil layers were determined as $1 \times 10^{-10}$, $1 \times 10^{-8}$, $1 \times 10^{-2}$, and $1 \times 10^{-2}$ m/s, respectively. The initial fluid balance was achieved within the allowable convergence value. The interface element was not introduced for the pile-soil interaction in the study. The steel pipe pile and its surrounding soft soil always stuck together even in situations involving large deformations. The flow and cohesion characteristics of the silt and mud were difficult to capture in the numerical modeling.

The fill was simulated in five lifts using the zone-type element with the elastic constitutive model. Young's modulus, the density, and Poisson's ratio of the fill were determined as $1.0 \times 10^7$ Pa, 1940 kg/m$^3$, and 0.3, respectively. The surcharge loading was then carried out by activating each plain fill layer in the same sequence of the field construction. The whole model was calculated to reach a balance state (i.e., both the force and fluid balance) after the placement of each new fill layer. Each lift was kept for three days, and then the next lift was placed. The gravity force of the fill layers was transferred to the underlying foundation soil and the steel pipe pile. The deformation of the foundation soil and the structure, the excess pore water pressure, and the earth pressure acting at the surface of the pile were recorded by writing the fish function and history command.

## 4. Results and Discussion

### 4.1. Model Verification

Figure 5 shows the horizontal displacements of the steel pipe pile at the ground surface measured by the field test and calculated by the proposed numerical model after each loading, respectively. The displacement of the numerical results during the first three lift loadings was in good agreement with the field results. The horizontal displacement of the steel pipe pile increased significantly in the fifth lift loading in the field test and even could not reach a stable state after three days' observation. The numerical results showed good convergence after the placement of each new lift. The maximum horizontal displacements calculated by the numerical model and the field test were 236.1 mm and 273.0 mm, respectively, at the end of the fifth lift loading. The maximum displacement calculated from the numerical model was 13.5% smaller than the field results. Figure 6 shows the horizontal displacements along the steel pipe pile obtained by the field test and numerical model, respectively, after the fifth lift loading. The field result was measured by the inclinometer tube in the field test. The shapes of the displacement profile were agreed upon between the field test and the numerical results, especially for the pile depth deeper than 20 m. Overall, the horizontal displacement behavior of the numerical model matched the field results from a practical point of view. The accuracy and reliability of the proposed numerical model were verified.
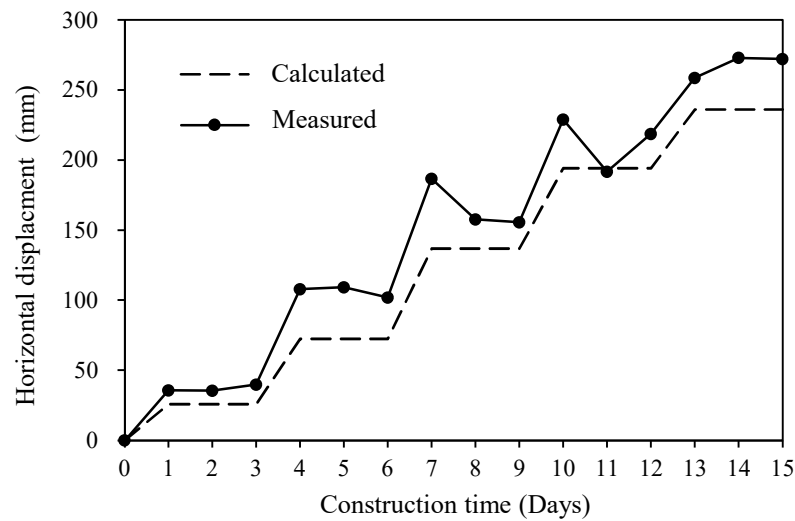
**Figure 5.** The comparison of the measured and calculated horizontal displacement of the pile at the ground surface.
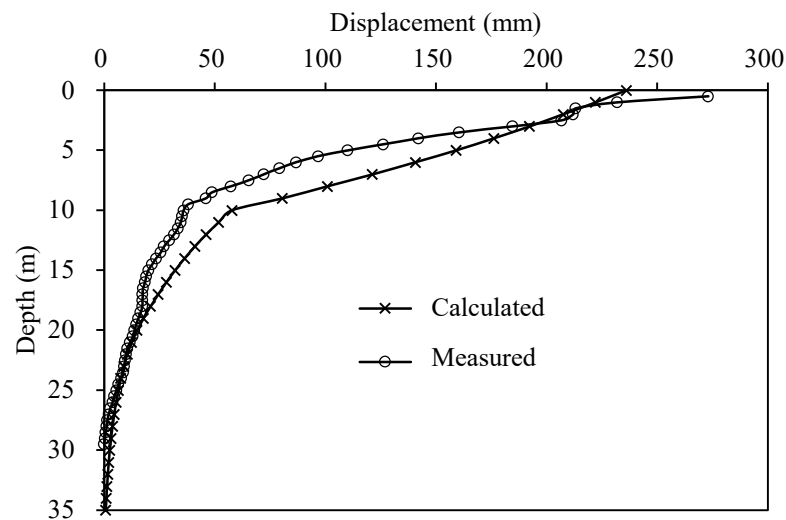


**Figure 6.** The horizontal displacements along the steel pipe pile obtained by the field test and numerical model.
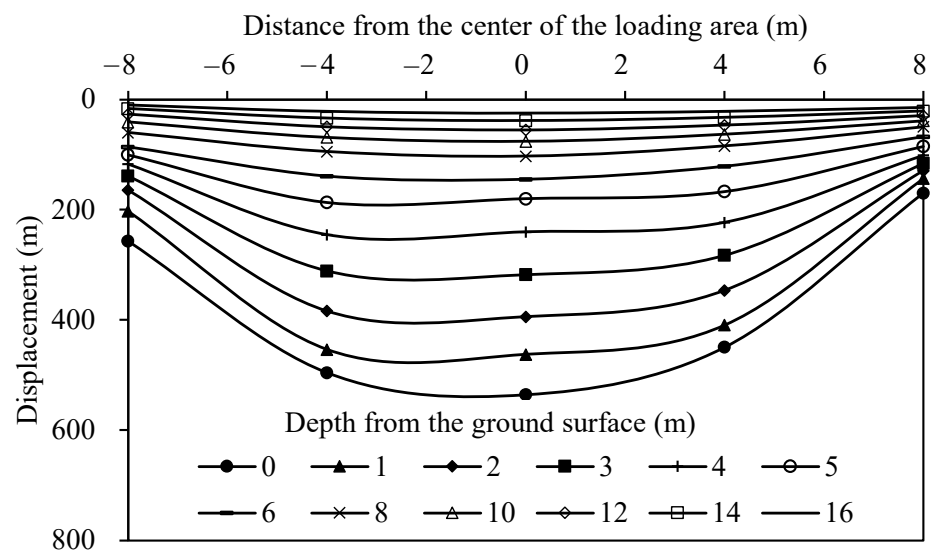
*4.2. The Vertical Displacement of the Foundation Soil*

　　Figure 7 shows the vertical displacement curves of the foundation soil at different depths below the loading area. The vertical displacement was calculated at the end of the 5th lift loading from the numerical model. Two sections were considered and shown in Figure 2. A-A section was the short edge of the loading area. B-B section was at the center of the loading area. As shown in Figure 7a, the center of the loading area developed downward displacement (i.e., positive settlement). The corner of the loading area developed upward displacement (i.e., uplift). The distribution of vertical displacement was symmetrical at the center of the loading area. The maximum uplift and settlement happened at the ground surface (i.e., the depth was 0 m). Their values were 74 mm and 110 mm, respectively. The distribution width of the settlement deformation was approximately 12 m in the center of the A-A section. The uplift deformation only happened within a shallow depth of 6 m. The vertical displacement of the foundation soil typically decreased with the increase in depth. The distribution of the vertical displacement was close to uniform for the depth deeper than 10 m. Due to the existence of the steel pipe pile, the vertical displacement of the soil adjacent to the pile (e.g., the uplift deformation) was slightly larger than that for the soil on the opposite side. For example, the vertical displacements of the soil at a depth of 0 m were

−82 mm and −74 mm, respectively, for the location adjacent to the pile and the location on the opposite side.
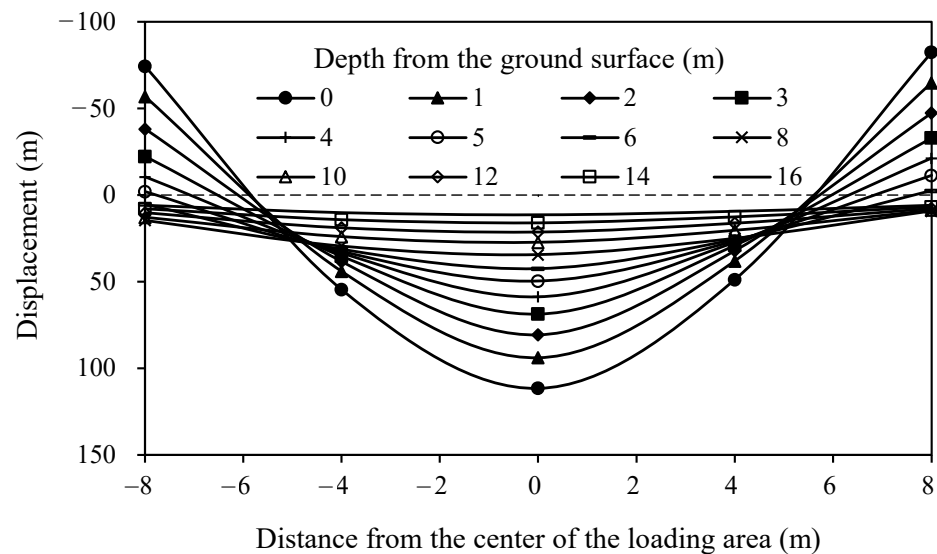


(**a**) A-A section



(**b**) B-B section

**Figure 7.** The vertical displacement curves of the foundation soil at different depths at: (**a**) A-A section; (**b**) B-B section.

　　　Figure 7b shows the vertical displacement curves of the foundation soil at the B-B section. The B-B section always developed downward displacement (i.e., the positive settlement) at different depths. The foundation soil at the center of the loading area developed more settlement than the foundation soil at the edge of the loading area. The maximum settlements were 535, 462, 394, 318, 240, 180, 144, 102, 76, 55, 38, and 25 mm for depths of 0, 1, 2, 3, 4, 5, 6, 8, 10, 12, 14 and 16 m, respectively. Settlement decreased with the increase in depth and showed uniform distribution for depths deeper than 10 m. Due to the constraint of the steel pipe pile, the settlement at the right edge (i.e., adjacent to the pile) was significantly smaller than the settlement at the left edge. For example, the vertical displacements of the soil at a depth of 0 m were 170 mm and 257 mm, respectively, at the right and the left edge. The vertical displacement of the foundation soil was constrained by the adjacent pile.

### 4.3. The Lateral Displacement of the Pile and the Foundation Soil

Figure 8 shows the distribution of the lateral displacement of the steel pipe pile along the depth. The displacement was calculated at the end of each lift loading from the numerical model. A large amount of displacement happened within a shallow depth of 10 m. The lateral displacement decreased with the increase in depth and increased with the placement of the new lift loading. The reduction rate of the lateral displacement was great when the depth was within 10 m. The maximum lateral displacements of the pile at the ground surface were 25.8, 72.5, 137.0, 194.3, and 236.1 mm after each loading, respectively.
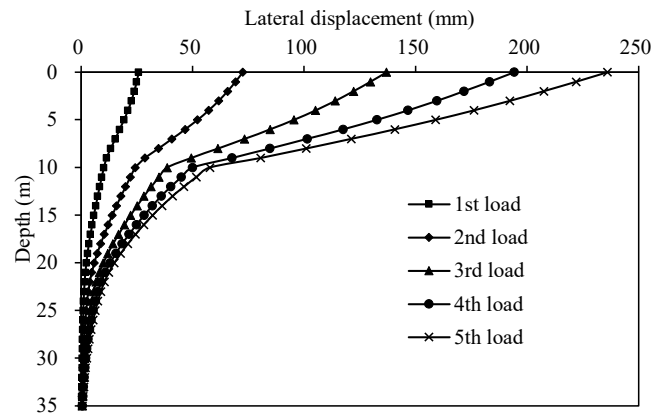
**Figure 8.** The lateral displacement of the steel pipe pile along the depth after each loading.

Figure 9 shows the distribution of the lateral displacement of the foundation soil at the end of the 5th lift loading. Six locations were marked in Figure 2. Their horizontal distances away from the center of the pile were 1, 6, 11, 16, 21, and 36 m, respectively. The distribution pattern of the lateral displacement of the foundation soil was different from that for the steel pipe pile. The maximum lateral displacement happening in relation to the depth varied from 1 to 4 m in different cases rather than the ground surface. The lateral displacement first increased to a maximum value with the increase in depth and then decreased to zero with the increase in depth. The lateral displacement was slight when the depth exceeded 30 m—the position of the maximum lateral displacement moved downward and was not on the ground surface. The maximum lateral displacement decreased with the increase in distance away from the center of the pile. The maximum lateral displacement of the foundation soil was 191.0, 153.0, 103.0, 28.6, 20.7, and 6.4 mm, respectively, for cases with horizontal distances of 1, 6, 11, 16, 21, and 36 m. Interestingly, the lateral displacement at the ground surface sharply decreased as the distance increased from 1 to 6 m. It can be concluded that the major influence zone of the lift loading was about 11 m in horizontal distance away from the center of the pile.
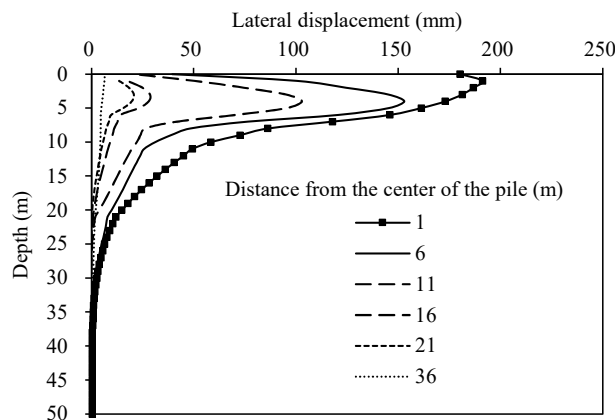
**Figure 9.** The lateral displacement of the foundation soil after the 5th loading.

*4.4. Excess Pore Water Pressure*

Figure 10 shows the variation of the excess pore water pressure (EPWP) with construction time at different depths. The EPWP was calculated based on the numerical model. For the purpose of brevity, only the location at the center of the surcharge loading region was investigated. The EPWP typically increased with the increase in depth, except for the location at a depth of 2 m. This location (at a depth of 2 m) was close to the water table (e.g., at a depth of 1 m) and the fill loading zone. Its EPWP increased rapidly and then dissipated to a low value after the placement of each new lift loading. The EPWP at a depth of 2 m was larger than those at depths of 4 m or even 6 m during loading. The EPWP typically increased with the elapse of the construction time except for the location at a depth of 2 m during each loading. The increments of EPWP at a depth of 2 m were 33.5, 23.5, 12.2, 7.9, and 4.7 kPa after each lift loading, respectively. The increment of EPWP at the depth of 4 m was 39.6, 15.2, 9.7, 6.4, and 3.7 kPa after each lift loading, respectively. The increment of EPWP at the depth of 6m was 51.8, 14.7, 10.5, 6.6, and 3.7 kPa after each lift loading, respectively. Increments of EPWP at a depth of 8 m were 65.2, 13.2, 10.6, 6.5, and 3.6 kPa after each lift loading, respectively. The increment of the EPWP was not linear with the increase of the applied surcharge loading. The initial EPWP increased significantly just after the placement of the 1st lift loading. Dissipation of the EPWP requires years to reach the full consolidation state due to the extremely low permeability coefficient of the soft foundation soil. It was obvious that a period of three days was not enough for the foundation soil to consolidate. The value of the EPWP continued to increase and accumulated with the placement of the new lift loading.
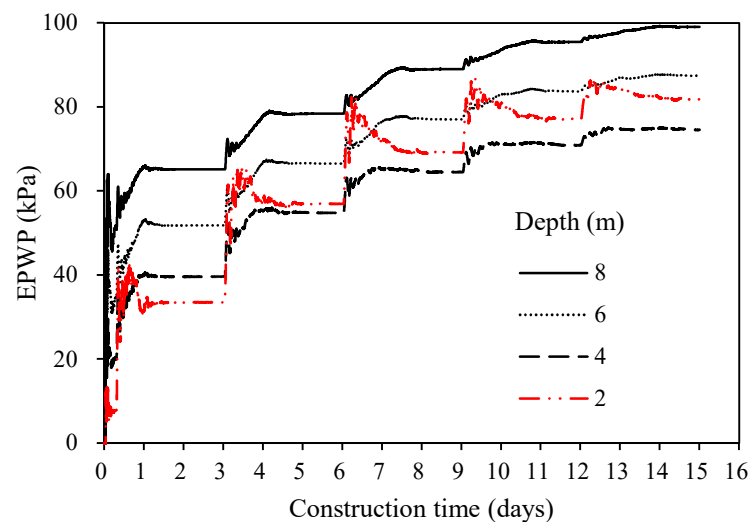


**Figure 10.** Variations in EPWP with construction time at the center of the surcharge loading region.

*4.5. Lateral Earth Pressure*

The lateral earth pressure was important for the understanding of the interaction effect and load transfer mechanism of the pile foundation constructed in extensively soft soil. The soil zone adjacent to the steel pipe pile was selected and its horizontal stress was the lateral earth pressure acting at the pile. Figure 11 shows the distribution of the lateral earth pressure under different lift loading. The lateral earth pressure typically increased with the increase of the depth at the end of the 1st lift loading. However, the lateral earth pressure within the shallow depth of 15 m decreased with the increase in surcharge load (i.e., at the end of the 3rd and 5th lift loadings). For soil deeper than 15 m, the change in lateral earth pressure with increases in surcharge loading was not significant. The distribution of lateral earth pressure in the shallow soil layer was complicated, and even a negative value of lateral earth pressure was developed under a high surcharge load. The positive value of the lateral earth pressure indicated that the soil and the pile contacted each other. The soil transferred the surcharge and lateral loads to the adjacent pile. The earth pressure at the

depth of 9 m decreased from 282.9 kPa at the end of the 1st lift loading to −291.1 kPa at the end of the 5th lift loading. The negative value of the lateral earth pressure indicated that the suction effect was dominant at the soil-pile interface. The decrease in lateral earth pressure in the shallow depth was also found in the centrifuge experiment [36] and in the numerical analysis [29]. The soil applied negative lateral earth pressure on the adjacent pile. It can be concluded that the negative lateral earth pressure only happened in a situation of high surcharge loads and extensive soil movement.
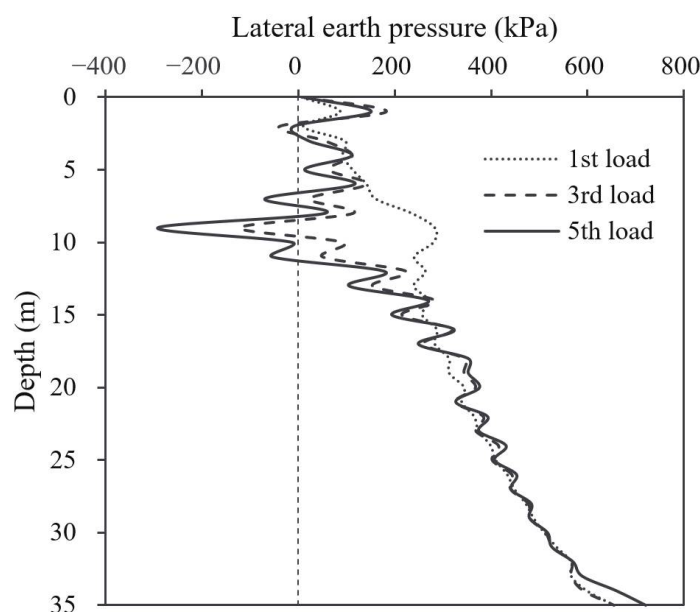


**Figure 11.** The distribution of the lateral earth pressure under different lift loading.

### 4.6. Variation of the m Value

Based on the hypothesis of the elastic foundation soil [37], the horizontal resistance ($\sigma_{zx}$) provided by the foundation soil can be calculated as follows:

$$\sigma_{zx} = Cx_z \tag{1}$$

where $C = mz$ was the horizontal resistance coefficient of soil (kN/m$^3$); $x_z$ was the horizontal displacement of the soil at a depth of $z$; and $m$ was the proportion coefficient of the horizontal resistance coefficient of soil (kN/m$^4$).

The determination of $m$ was complicated and challenging in the field. The design code in many countries and regions only provided empirical values for the geotechnical applications. The $m$ value changed significantly with different types of soil and varied with the depth of the soil. Reasonable determination of the $m$ value was essential for the design of laterally loaded structures, especially in the extensively soft soil. The numerical method provided an alternative approach to investigating the variation of the $m$ value and was presented in this study. The horizontal resistance along the pile in this study was the lateral earth pressure acting at the surface of the steel pipe pile. The value and distribution of the horizontal resistance were presented in Figure 11. The horizontal displacement of the soil can be drawn from the numerical model. Therefore, the variation of the $m$ value with depth was calculated based on Equation (1).

Figure 12 shows the distribution of the $m$ value along the piles at the end of different lift loadings. The calculated $m$ value was compared with the recommended $m$ value from the technical code for building pile foundations in China (JGJ 94-2008). The recommended values of m for the silt and mud soil were between 2 and 4.5 MN/m$^4$. It was clear that the values of $m$ decreased with the increase in depth. The $m$ value in the shallow soil layer was typically smaller than the lower limit of the recommended value (e.g., 2 MN/m$^4$) due to

the large lateral displacement of the foundation soil. The $m$ value in the deep soil layer was significantly higher than the upper limit of the recommended value (e.g., $4.5 \, \text{MN/m}^4$) because of the small lateral displacement and the high earth pressure of the foundation soil. The design code may overestimate the horizontal resistance of the shallow foundation soil, which was dangerous for the laterally loaded structures.
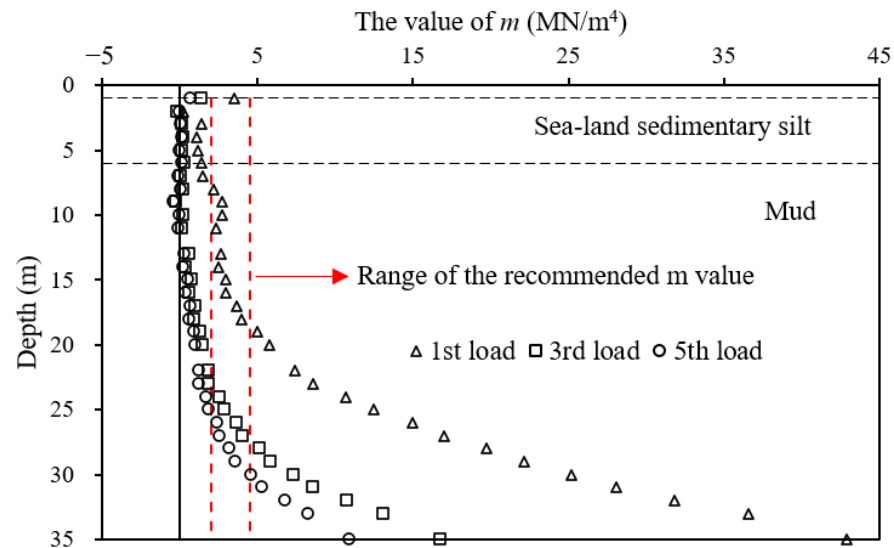


**Figure 12.** The distribution of the $m$ value along the depth after the 1st, 3rd, and 5th loadings.

Figure 12 also shows that the value of $m$ decreased with the increase of the surcharge loads. Higher surcharge loads caused larger lateral displacement of the pile and the foundation soil. The $m$ value at the end of the 5th lift loading was smaller than the lower limit of the recommended value (e.g., $2 \, \text{MN/m}^4$) until the depth reached 25 m. The average $m$ values along the depth were 11.4, 3.5, and $2.2 \, \text{MN/m}^4$, respectively, at the end of the 1st, 3rd, and 5th loadings. The horizontal resistance of the shallow foundation soil at a high surcharge load (i.e., caused large lateral displacement) was further overestimated by the design code. Attention should be given for the design and analysis of the laterally loaded structures in such geotechnical situations.

## 5. Conclusions

In this paper, the finite difference (FD) numerical method was used to investigate the behavior of the steel pipe pile constructed in extensively soft soil under high lateral loads. The vertical and lateral displacement of the foundation soil and pile, the excess pore water pressure (EPWP), the lateral earth pressure, and the proportion coefficient of the horizontal resistance coefficient of soil ($m$) were analyzed using the proposed numerical model. The following conclusions can be drawn:

(1) The corner of the loading area developed large uplift deformation. The uplift deformation only happened within a shallow depth of 6 m for the foundation soil at the short edge of the loading area. The foundation soil at the center section always developed downward displacement at different depths.

(2) The pile developed large lateral displacement for a shallow depth of 10 m. The lateral displacement decreased sharply with the increase in depth and increased with the placement of the new lift loading. The foundation soil developed the maximum lateral displacement at depths varying from 1 to 4 m in different cases instead of the ground surface. The lateral displacement of the soil was slight when the depth exceeded 30 m.

(3) The EPWP initially increased significantly after the placement of the 1st lift loading. The increment of the EPWP was not linear with the increase of the surcharge load. The value of the EPWP continued to increase and accumulated with the placement of the new lift loading.

(4)　The lateral earth pressure typically increased with the increase in depth at the end of the 1st lift loading. The distribution of the lateral earth pressure in the shallow soil layer was complicated and a negative value was observed under a high surcharge load. The suction effect could be dominant at the soil-pile interface in the situation of high surcharge load and large soil movement.

(5)　The *m* value in the shallow soil layer was typically smaller than the lower limit of the recommended value, while the *m* value in the deep soil layer was significantly higher than the upper limit of the recommended value. The value of *m* decreased with the increase of the surcharge load. The design code overestimated the horizontal resistance of the shallow foundation soil at a high surcharge load and large lateral displacement.

**Author Contributions:** Conceptualization, M.G. and Q.F.; methodology, M.G.; software, X.C.; validation, X.C. and H.L.; formal analysis, X.C. and H.L.; investigation, X.W. and B.M.; resources, X.W. and B.M.; writing—original draft preparation, X.C.; writing—review and editing, Q.F.; supervision, M.G.; project administration, M.G.; funding acquisition, M.G. and Q.F. All authors have read and agreed to the published version of the manuscript.

**Institutional Review Board Statement:** Not applicable.

**Informed Consent Statement:** Not applicable.

**Data Availability Statement:** Some or all data, models, or code generated or used during the study are available from the corresponding author by request.

**Conflicts of Interest:** The authors declare that the research was conducted in the absence of any commercial or financial relationships that could be construed as potential conflicts of interest.

## References

1.　Springman, S.M.; Ellis, E.A. Full-height piled bridge abutments constructed on soft clay. *Géotechnique* **2001**, *3*, 3–14.
2.　Li, H.; Liu, S.; Yan, X.; Gu, W.; Tong, L. Effect of loading sequence on lateral soil-pile interaction due to excavation. *Comput. Geotech.* **2021**, *134*, 104134. [CrossRef]
3.　Poulos, H.G. Analysis of piles in soil undergoing lateral movement. *J. Soil Mech. Found. Div.* **1973**, *391*, 391–406. [CrossRef]
4.　Gu, M.; Han, J.; Zhao, M. Three-dimensional discrete-element method analysis of stresses and deformations of a single geogrid-encased stone column. *Int. J. Géoméch.* **2017**, *17*, 04017070. [CrossRef]
5.　Gu, M.; Han, J.; Zhao, M. Three-dimensional DEM analysis of single geogrid-encased stone columns under unconfined compression: A parametric study. *Acta Geotech.* **2017**, *12*, 559–572. [CrossRef]
6.　Gu, M.; Mo, H.; Qiu, J.; Yuan, J.; Xia, Q. Behavior of floating stone columns reinforced with geogrid encasement in model tests. *Front. Mater.* **2022**, *9*, 980851. [CrossRef]
7.　Springman, S.M. Lateral Loading on Piles due to Simulated Embankment Construction. Ph.D. Thesis, University of Cambridge, Cambridge, UK, 1989.
8.　Yuan, B.; Chen, W.; Zhao, J.; Li, L.; Liu, F.; Guo, Y.; Zhang, B. Addition of alkaline solutions and fibers for the reinforcement of kaolinite-containing granite residual soil. *Appl. Clay Sci.* **2022**, *228*, 106644. [CrossRef]
9.　Yuan, B.; Li, Z.; Chen, W.; Zhao, J.; Lv, J.; Song, J.; Cao, X. Influence of groundwater depth on pile-soil mechanical properties and fractal characteristics under cyclic loading. *Fractal Fract.* **2022**, *6*, 198. [CrossRef]
10.　Gu, M.; Cui, J.; Yuan, J.; Wu, Y.; Li, Y.; Mo, H. The stress and deformation of stone column-improved soft clay by discrete element modelling. *Eur. J. Environ. Civ. Eng.* **2020**, *26*, 1544–1560. [CrossRef]
11.　Gu, M.; Han, J.; Zhao, M. Three-dimensional DEM analysis of axially loaded geogrid-encased stone column in clay bed. *Int. J. Géoméch.* **2020**, *1–11*, 04019180. [CrossRef]
12.　Gu, M.; Zhao, M.; Zhang, L.; Han, J. Effects of geogrid encasement on lateral and vertical deformations of stone columns in model tests. *Geosynth. Int.* **2016**, *23*, 100–112. [CrossRef]

13.   Al-Abboodi, I.; Sabbagh, T.T.; Al-Salih, O. Response of passively loaded pile groups—An experimental study. *Geomech. Eng.* **2020**, *333*, 333–343.

14.   Karkush, M.O.; Aljorany, A.N.; Jaffar, G.S. Behavior of passive single pipe pile in sandy soil. *IOP Conf. Ser. Mater. Sci. Eng.* **2020**, *737*, 012106. [CrossRef]

15.   Karkush, M.O.; Jaffar, G.S. Simulation the behavior of passive rigid pile in sandy soil. *J. Eng. Technol. Sci.* **2020**, *52*, 449–467. [CrossRef]

16.   Yuan, B.; Chen, M.; Chen, W.; Luo, Q.; Li, H. Effect of pile-soil relative stiffness on deformation characteristics of the laterally loaded pile. *Adv. Mater. Sci. Eng.* **2022**, *2022*, 1–13. [CrossRef]

17.   Sabbagh, T.T.; Alsalih, O.; Al-Abboodi, I. Experimental investigation of batter pile groups behaviour subjected to lateral soil movement in sand. *Int. J. Geotech. Eng.* **2019**, *14*, 705–716. [CrossRef]

18.   Bellezza, I. Closed-form expressions for a rigid passive pile in a two-layered soil. *Géotechnique Lett.* **2020**, *10*, 242–249. [CrossRef]

19.   Ramalakshmi, M. Force-displacement response of bridge abutments under passive push. *Mater. Today Proc.* **2020**, *43*, 883–887. [CrossRef]

20.   Zhang, H.; Shi, M.; Guo, Y. Semianalytical solutions for abutment piles under combined active and passive loading. *Int. J. Géoméch.* **2020**, *20*, 04020171. [CrossRef]

21.   Zhang, H.; Shi, M.; Yang, L.; Guo, Y. A semianalytical solution for passively loaded piles adjacent to surcharge load. *Adv. Civ. Eng.* **2020**, *2020*, 1–19. [CrossRef]

22.   Cole, R.T. Full-Scale Effects of Passive Earth Pressure on the Lateral Resistance of Pile Caps. Ph.D. Thesis, Brigham Young University, Provo, UT, USA, 2003.

23.   Tavenas, F.; Mieussens, C.; Bourges, F. Lateral displacements in clay foundations under embankments. *Can. Geotech. J.* **1979**, *16*, 532–550. [CrossRef]

24.   Poulos, H.G. Difficulties in prediction of horizontal deformations of foundations. *J. Soil Mech. Found. Div.* **1972**, *98*, 843–848. [CrossRef]

25.   Li, H.-Q.; Wei, L.-M.; Feng, S.-Y.; Chen, Z. Behavior of piles subjected to surcharge loading in deep soft soils: Field tests. *Geotech. Geol. Eng.* **2019**, *37*, 4019–4029. [CrossRef]

26.   Nicu, N.D.; Antes, D.R.; Kessler, R.S. Field measurements on instrumented piles under an overpass abutment. Highway research record. In Proceedings of the 50th Annual Meeting of the Highway Research Board, Washington, DC, USA, 18–22 January 1971; pp. 90–102.

27.   Chai, J.; Ong, C.; Carter, J.; Bergado, D. Lateral displacement under combined vacuum pressure and embankment loading. *Géotechnique* **2013**, *63*, 842–856. [CrossRef]

28.   Ellis, E.; Springman, S. Modelling of soil–structure interaction for a piled bridge abutment in plane strain FEM analyses. *Comput. Geotech.* **2001**, *28*, 79–98. [CrossRef]

29.   Yang, M.; Shangguan, S.; Li, W.; Zhu, B. Numerical study of consolidation effect on the response of passive piles adjacent to surcharge load. *Int. J. Géoméch.* **2017**, *17*, 04017093. [CrossRef]

30.   Al-abboodi, I.; Sabbagh, T.T. Numerical modelling of passively loaded pile groups. *Geotech. Geol. Eng.* **2019**, *37*, 2747–2761. [CrossRef]

31.   Zhang, H.; Sun, K. Influence of surcharge load on the adjacent pile foundation in coastal floodplain. *Insight-Civ. Eng.* **2020**, *3*, 17–25. [CrossRef]

32.   Abo-Youssef, A.; Morsy, M.S.; ElAshaal, A.; ElMossallamy, Y.M. Numerical modelling of passive loaded pile group in multilayered soil. *Innov. Infrastruct. Solut.* **2021**, *6*, 1–13. [CrossRef]

33.   Yi, S.; Liu, J. Field investigation of steel pipe pile under lateral loading in extensively soft soil. *Front. Mater.* **2022**, *9*, 480. [CrossRef]

34.   Kelesoglu, M.; Springman, S. Analytical and 3D numerical modelling of full-height bridge abutments constructed on pile foundations through soft soils. *Comput. Geotech.* **2011**, *38*, 934–948. [CrossRef]

35.   *FLAC3D 6.0 Document*; Itasca Consulting Group: Minneapolis, MN, USA, 2018.

36.   Bransby, M.; Springman, S. 3-D finite element modelling of pile groups adjacent to surcharge loads. *Comput. Geotech.* **1996**, *301*, 301–324. [CrossRef]

37.   Winkler, E. *Die Lehre von Elastizitat und Festigkeit (The Theory of Elasticity and Stiffness)*; H. Domenicus: Prague, Czech Republic, 1867.